Applied Surface Science 400 (2017) 24–37

Contents lists available at ScienceDirect

Applied Surface Science

journal homepage: www.elsevier.com/locate/apsusc

Full Length Article

Improved adaptability of polyaryl-ether-ether-ketone with texture pattern and graphite-like carbon film for bio-tribological applications

Siming Ren[a,c], Jinxia Huang[b], Mingjun Cui[b,c], Jibin Pu[a,*], Liping Wang[a,*]

[a] Key Laboratory of Marine Materials and Related Technologies, Key Laboratory of Marine Materials and Protective Technologies of Zhejiang Province, Ningbo Institute of Materials Technology and Engineering, Chinese Academy of Sciences, Ningbo 315201, China
[b] State Key Laboratory of Solid Lubrication, Lanzhou Institute of Chemical Physics, Chinese Academy of Science, Lanzhou 730000, PR China
[c] University of Chinese Academy of Sciences, Beijing 100039, China

ARTICLE INFO

Article history:
Received 28 July 2016
Received in revised form
10 December 2016
Accepted 19 December 2016
Available online 21 December 2016

Keywords:
Polyaryl-ether-ether-ketone
Graphite-like carbon
Texture surface
Biological solution

ABSTRACT

With the development of surface treatment technology, an increasing number of bearings, seals, dynamic friction drive or even biomedical devices involve a textured surface to improve lubrication and anti-wear. The present investigation has been conducted in order to evaluate the friction and wear behaviours of textured polyaryl-ether-ether-ketone (PEEK) coated with a graphite-like carbon (GLC) film sliding against stainless steel pin in biological medium. Compared with pure PEEK, the PEEK coated with GLC film shows excellent tribological performance with a low friction of 0.08 and long lifetime (wear volumes are about 3.78×10^{-4} mm^3 for un-textured one and 2.60×10^{-4} mm^3 for textured GLC film after 36,000 s of sliding) under physiological saline solution. In particular, the GLC film with appropriate dimple area density is effective to improve friction reduction and wear resistance properties of PEEK substrate under biological solution, which is attributed to the entrapment of wear debris in the dimples to inhibit the graphitization and the fluid dynamic pressure effect derived from the texture surface to increase the thickness in elastohydrodynamic lubrication (EHL) film during sliding motions. Moreover, the friction coefficient of GLC film under physiological saline solution decreases with the increase in the applied load. With the increasing applied load, the texture surface is responsible for accounting the improved wear resistance and a much lower graphitization of the GLC film during whole test.

1. Introduction

Biological synovial joints, e.g., hip, knee or shoulder joints, are complex and delicate structures capable of lubrication, damping, wear resistance and some other functions [1,2]. The excellent performance is due to the optimized combination of articular cartilage, a load-bearing connective tissue covering the bones involved in the joint and synovial fluid to protect bone-injury [3]. Unfortunately, osteoarthritis or degenerative joint diseases are caused by aging or repetitive injury, which can lead to damage of cartilage and bone [4]. Hence, transplantating prosthetic joint into bone can achieve a relief of pain and improve the joint mobility. However, the biocompatibility between living tissues and non-living materials is the critical factor that limits the lifetime of implant materials [5]. In a historical and a practical perspective, a broad range of interactive behaviour occurs between tissues and prosthesis (metal or alloy) for substitution of hip and knee joints, and some wear debris particles may be generated in the human body to trigger a series of adverse biological reactions during this process, thus leading to the premature failure of the prosthesis [6,7].

Polyaryl-ether-ether-ketone (PEEK), one of the polymers as substitute for metal alloy in implant replacement [8], exhibits the desirable mechanical properties, high thermal stability, wear and chemical resistance, no toxicity as well as high resistance to gamma irradiation [9–11]. In particular, PEEK has an advantage that the stiffness is much closer to the cortical bone in contrast to metals, ceramics or other polymers, thus reducing the effects of stress shielding after implantation [12,13]. Recent research has also investigated the bio-tribology of PEEK composites as bearing materials and flexible implants used for joint arthroplasty and spine patients [14,15]. Wang et al. have investigated carbon fiber reinforced PEEK composites as bearing surfaces for total joint replacements [14]. It is found that those composites offer a far superior wear resistance compared with ultrahigh molecular weight polyethylene (UHMWPE). Moreover, Kurtz and Devine review the history of how

* Corresponding authors.
E-mail addresses: pujibin@nimte.ac.cn (J. Pu), wangliping@nimte.ac.cn (L. Wang).

http://dx.doi.org/10.1016/j.apsusc.2016.12.159
0169-4332/

PEEK biomaterials come to be increasingly accepted for spine and orthopaedic implants over other high-performance thermoplastics [16]. Nevertheless, reduction of wear is still a major challenge in PEEK research as wear particles are responsible for early loosening of prosthetic devices [8,17]. Currently, graphite-like carbon (GLC) films have been applied in biomedicine due to its low friction and specific wear rate as well as good chemical inertness [18,19]. Moreover, it is well known that medical implants not only experienced the wear from relative motion between bone joints but also subjected to the degradation through the physiological fluids [20,21]. While many authors have addressed that the GLC film has a good compatibility with different types of cells like macrophages, fibroblasts, human myeloblasts, osteoblasts, and so on [13,22]. Thus, GLC film would be one of the optimum candidates for the modification of PEEK.

To improve the prevention of inflammatory and allergic reactions of the GLC film, many researchers have adopted doping metal or non-metal elements in amorphous carbon matrix [23,24]. In this paper, we deposit GLC film on the textured PEEK surface to improve the bio-tribological performance, since the regularly distributed texture surface can generate fluid dynamic pressure effect to increase the carrying capacity of film [25], store lubricating medium to prevent interlocking between contact surfaces [26], and capture the wear debris to reduce abrasive wear [27], thus effectively improving the lifetime and reliability of GLC film. Moreover, laser surface texturing (LST) has been applied to the PEEK surface treatment for bio-tribological applications owing to its versatility, fast adaptability, high precision and cleanness of environment [28]. Kovalchenko et al. have reported that the tribological properties can be significantly improved by LST technology textured steel surfaces [29]. He et al. also verify that appropriate dimple area density by LST technology is effective in enhancing reducing-friction property of titanium alloys substrate under air friction and liquid lubrication conditions [30]. However, the synergistic effect of GLC film and surface texturing on the tribological properties of PEEK under biological medium has not received enough attention and extensive research.

In previous works [21,31], our team has systematically investigated the bio-tribological performance and friction mechanism of PEEK coated with metal or non-metal doping GLC films under biological media. A fundamental aspect of this work is to utilize the texturing design to optimize the bio-tribological performance of GLC film in biological lubricant. The possible friction reduction and wear resistance mechanisms are discussed by probing into the effect of dimple density and applied load on the bio-tribological behaviour of un-textured and textured GLC films. The present paper takes the first step of a wide program and the final objective is to apply the textured GLC film on human joint.

2. Experimental section

2.1. LST of PEEK substrates

The specimens, with a dimension of Ø25 mm × 3 mm, were cut from bulk semi-crystalline PEEK rod and subsequently polished with different grades of diamond paste to obtain a surface roughness of $R_a \leq 140$ nm. Micro-dimple patterns were then created on the surfaces of PEEK substrates through a neodymiumyttrium aluminum garnet laser with a wavelength of 1064 nm, pulse width of 4 ns, spot diameter about 40 μm, using a frequency of 10 kHz and 90% overlapping rate of laser spot, and the specimens were processed with an average power of 10 W at a 5 mm/s traverse speed. After laser texturing, a gentle polishing process was used to remove bulges or burrs around the rim of the dimples. Two dimple area densities were fabricated with the same dimple geometric parameters and labeled as PEEK-T15% and PEEK-T30%, respectively.

2.2. Deposition of GLC film

Prior to deposition, all specimens were ultrasonically cleaned in acetone and alcohol for 20 min and then cleaned with Ar+ ions at a substrate pulsed bias of −500 V in sequence before. The GLC films on the textured and smooth PEEK substrates were obtained by unbalanced magnetron sputtering technique in a multi-target PVD system. Before the deposition of GLC film, Si interlayer was deposited with a Si target in order to enhance the adhesion between the substrate and film. Subsequently, one graphite target (purity 99.95%) with dimensions of $6 \times 76 \times 153$ mm^3 for sputtering carbon was used. A base pressure of 2.0×10^{-3} Pa in the chamber was attained with a turbomolecular pumping system, and then the total pressure was set at a pressure of 0.6 Pa by Ar inflation with a flow rate of 120 sccm. As the pressure of the vacuum chamber was reached, PEEK substrates were sputtered in situ for 15 min with argon plasma at a DC bias voltage of −1000 V and a duty cycle of 50%. Meanwhile, the rotation speed of PEEK substrate was 5 rpm during the deposition process. Finally, GLC film was deposited at a DC current of 1.2 A and a bias voltage of −300 V. Two dimple area densities of 15% and 30% were achieved. The corresponding specimens were labeled as GLC-T15% and GLC-T30%, respectively. The total deposition process lasted for 100 min. The process flow diagram of textured GLC film was shown in Fig. S1 in Supporting information.

2.3. Characterization

The surface topography and cross-sectional micrograph of the as-deposited GLC films were examined by field emission scanning electron microscopy (FESEM, JSM-6701F). Atomic force microscopy (AFM, Benyuan CSPM 4000) with contact mode was used to measure the surface roughness of the GLC film. The nanohardness (H) and Young's modulus (E) of PEEK and as-deposited GLC film were determined by the Nanotest600 nanoindenter apparatus (Micro Materials Ltd.), the indentation depth was about 10% of the film thickness for GLC and 100 nm for PEEK substrate. The chemical states of as-deposited GLC film were analyzed by a PHI-5702 multifunctional X-ray photoelectron spectroscope (XPS) made by American Institute of Physics Electronics Company using K-Alpha irradiation as the excitation source. The binding energies of the target elements were determined at a pass energy of 29.3 eV, with a resolution of about ±0.3 eV, using the binding energy of contaminated carbon (C1s: 284.8 eV) as the reference. The morphology and depth of textured GLC film were measured using a MicroXAM 3D surface profiler. The microstructure of as-deposited GLC-smooth and textured GLC films were characterized by Raman spectroscopy equipped with a 532 nm argon ion laser (Raman, HR800 Raman spectroscopic measurement). The wear tracks of GLC films were checked by scanning electron miscroscopy (SEM, EVO18, ZEISS, Germany).

2.4. Tribological test

A CSM tribometer in the pin-on-plate reciprocating sliding was used for preliminary materials evaluation by friction and wear testing. The amplitude was 5 mm, and sliding frequency was 6.37 Hz corresponding to a velocity of 10 cm s^{-1}. The load of 3 N was applied through a stationary loading system. A 316L stainless steel pin with ball head (6 mm in diameter and surface roughness (R_a) value of 0.02 μm) was employed as counterpart, and the sliding direction was parallel to the LST patterns. The ambient temperature and relative humidity were 23 ± 2 °C and 23 ± 5%, respectively. Two

series of tribological tests, including those in air friction and liquid lubrication conditions, were run for 120 min with the same test parameters. The dry friction was tested in ambient air, and the liquid friction was performed in physiological saline (PS) or fetal bovine serum (FBS) biological lubricant. Commercial FBS lubricating medium (protein concentration was about 4.3% w/v) was used to simulate body fluid. During the wet friction process, two droplets of the biological solution were spreaded on the contact surface before the mating steel pin was brought in contact. The friction coefficient was continuously recorded during testing, and the mentioned friction coefficient in this paper was the mean friction coefficient. The average friction was measured at three times under the same tested condition to calculate the average value and the error bar was calculated from the standard deviation. After friction test, the depth of wear track was measured using a surface profiler (Alpha-step D-100) and each wear track was measured three to five measurements to insure the repeatability of results.

3. Results and discussion

3.1. Film structure analysis

GLC film displays a uniformly dense surface with nanometer-sized particles as shown in Fig. 1a. Fig. 1b shows a cross-sectional SEM image of GLC film on PEEK substrate, in which the thickness of GLC film and Si interlayer is about 1.76 μm and 275 nm, respectively. As shown in the cross-sectional image, the GLC film has a homogeneous and dense microstructure. The AFM image of GLC film shown in Fig. 1c indicates that the film composed of small spheres has a relatively rough and compact surface (R_a = 113 nm) which is related to the rough surface of PEEK substrate. The chemical composition and bonding identification of as-deposited GLC film are investigated by XPS analysis, as shown in Fig. 2. Full-scale XPS spectra of GLC give a composition of 82.78 at.% C and 17.22 at.% O. In order to further analyze the chemical states, C 1 s spectrum is fitted by Guassian-Lorentian function. The C 1 s spectrum can be fitted into three distinct carbon species: C=C species (sp^3) at 284.4 eV, C—C species (sp^2) at 285.3 eV, C—O or C=O species at 286.5 eV, respectively [32–34]. Based on the fitted results of C 1 s spectrum, the ratio of sp^3 to sp^2 is around 0.75, which indicates the film has a high fraction of sp^2-C constituents. It confirms that the as-deposited GLC film is dominated by the amorphous graphite-like structure.

The morphology and depth of textured GLC film are measured using a MicroXAM 3D surface profiler. As shown in Fig. 3, the textured GLC film has a homogeneous and dense microstructure, and no obvious defects. The micro-dimple of GLC-T15% and GLC-T30% are about 300 μm in diameter with an average depth of 100 μm. Fig. 4 shows the Raman spectra of GLC-T30% film outside and inside the dimple. A broad asymmetric Raman scattering band is observed from 800 to 2000 cm^{-1}. Results of Raman analysis show that the film in different locations (including the outside and inside dimple) has similar structure, typical of graphite-like structure [35,36]. Moreover, the fitted Raman spectra gives the strong confirmation of amorphous graphite-like structure in as-deposited GLC film, which is supported by an I_D/I_G intensity ratio of 2.82 for outside and 2.85 for the inside dimple. And a narrowing G peak with a FWHM (full widths at half maximum) is about 137.5 and 139.2 cm^{-1} for the outside and inside of dimple. The G-band for the outside and inside dimple is located at 1570 and 1572 cm^{-1}, respectively.

3.2. Friction and wear behaviours of textured and un-textured PEEK

Fig. 5 shows the friction curves and average coefficient of friction (COF) for un-textured and textured PEEK against the stainless steel pin in three lubrication conditions. In the air (Fig. 5a), the friction curves of PEEK with texture density of 30% and 15% are relatively steady, whereas the PEEK without texture presents a tendency that the increases with the sliding time and eventually the value of COF is higher than that of textured PEEK. This higher COF may be attributed to the adhesion effect between the polymer surface and stainless steel pin during friction process [37]. In case of the textured PEEK, wear debris can be captured to alleviate the adhesion effect. In PS medium, COF is fluctuant over the whole experimental process (Fig. 5b), especially for the un-textured PEEK: the COF increases dramatically after sliding time of 3600 s; whereas in the FBS (Fig. 5c), the friction curves of textured PEEK have a similar trend to air environment that the COF is relatively stable and lower than that of the specimen without lubricating condition (Fig. 5a and d). Moreover, the value of COF for un-textured PEEK in the FBS solution is located between those of the textured PEEK density of 15% and 30%, which increases first and decreases afterward with increase in sliding time. From the mentioned average COF (Fig. 5d), it is interesting that the COF of PEEK with texture density of 15% is lower than that of 30%. The results illustrate the appropriate texture density can effectively reduce the COF, whereas the high texture density will cause the increased COF due to the increased surface roughness.

Fig. 6 shows the wear tracks and cross-section profiles of textured and un-textured PEEK in different medium. In air condition, the wear track is narrow, and severe adhesion behaviour occurs due to the increasing temperature of local area during sliding cycle. However, the adhesive wear can be alleviated for the textured PEEK because the micro-dimples can capture the wear debris during sliding cycle. The wear track of PEEK with deep groove in PS solution is wider than that in air condition, and the adhesion behaviour of polymer does not occur. This is because the surface roughness of PEEK is high and the viscosity of PS is low, which causes it difficult to form the effective and continuous elastohydrodynamic lubrication (EHL) film to cover the asperity of contact surface. Thus, the friction state in PS solution is a mixing state. From the microscopic scale angle, the contact surfaces at instantaneous moment exist both of solid-solid contact zone and fluid lubricated zone. When the tribopair is immersed in FBS solution, the wear track of PEEK is relatively shallower and narrower than that in PS solution. More importantly, there is a sharp contrast for the depth of wear tracks shown in Fig. 6b, where serious plough and wear grooves are distinguishable from biological solutions but absent in air condition. Since the biological solution hinders the modification of the counterpart by the transfer film from polymer debris, leading to a higher wear of PEEK than that in air condition [13,38]. However, PEEK has a comparatively shallow wear track in air condition, where a thermally induced mobile layer on the contact interface acts as a lubricant and reduces the wear of PEEK [39].

3.3. Friction and wear behaviours of textured and un-textured GLC films

Fig. 7 presents the friction curves and average COF of GLC film with different texture density in different medium. In general, there is a distinct decrease for the COF of GLC coated PEEK as a comparison with uncoated PEEK (Fig. 5d) at the same condition, regardless of with or without texture structure. For instance, the COF is fluctuant dramatically from 0.08 to 0.45 for the PEEK-T30% whereas it is fluctuant slightly from 0.08 to 0.12 for the GLC-T30% in PS solution. In air condition (Fig. 7a), the COF of textured GLC film increases sharply after 2000 s of sliding and then tends to be relatively stable after 3500 s, which indicates the film has been worn off locally. On the contrary, the un-textured GLC film plays a significant role in lubrication before 3500 s and then the COF increases with the increasing sliding time. When the specimen is tested in the biolog-

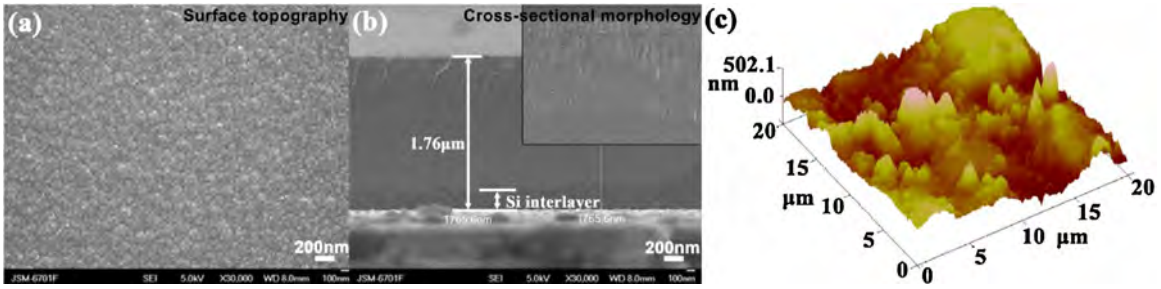

Fig. 1. (a) Surface, (b) cross-sectional and (c) AFM images of GLC films, the inset image in Fig. 1b is the magnified photos of cross-sectional image.

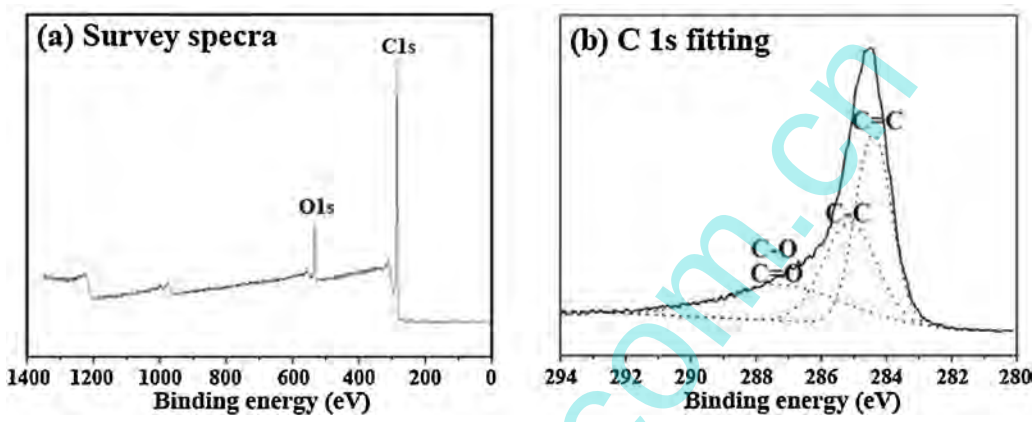

Fig. 2. (a) XPS spectra and (b) C 1s spectrum of as-deposited GLC film on the un-textured substrates.

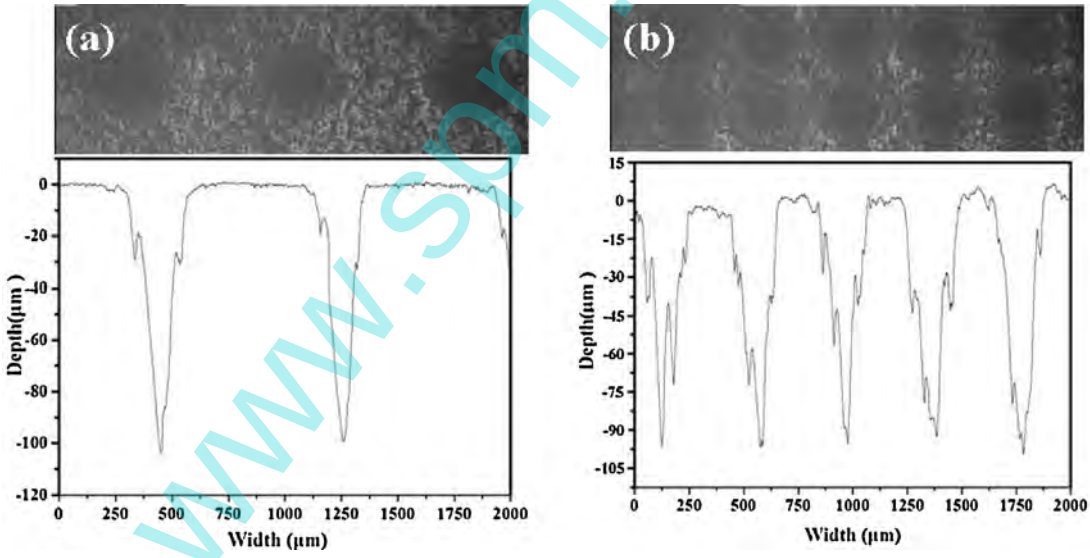

Fig. 3. The morphology and depth of textured GLC film with the pattern of micro-dimples, (a) GLC-T15% and (b) GLC-T30%.

ical medium, the COF of all specimens is low at the initial stage, then rises slowly with increasing sliding time and stabilizes eventually. In case of PS solution (Fig. 7b), the friction curves of GLC film exhibit the fluctuation during the whole sliding test, which is similar to that of PEEK (Fig. 5b). The fluctuant friction curve can be attributed to the combined effect of the chemicals in PS solution, friction force and possible rise of temperature [31]. For FBS solution (Fig. 7c), viscous protein sticks to the sliding surface of the film, and thus, the initial COF is relatively low. But with the increasing sliding cycle, the lubricating proteinaceous film gradually becomes thin and dense so that the COF rises at first and then becomes stable. The variations of friction curves are almost identical for both GLC-T15% and GLC-T30% films. Moreover, the COF of un-textured GLC film is much higher than that of the textured GLC film in PS and FBS solutions, as shown in Fig. 7d, suggesting that the texture structure plays a vital role in the solid-liquid composite lubricating effect.

Fig. 8 shows the wear tracks and cross-section profiles of textured and un-textured GLC films in different medium. Some grooves and spalling appear at the wear track of specimen in air condition, and the un-textured GLC film exhibits the highest spalling and widest wear track than that of others. Compared to uncoated PEEK in air condition (Fig. 6b), the wear track of GLC coated PEEK becomes wider and deeper, where the wear track

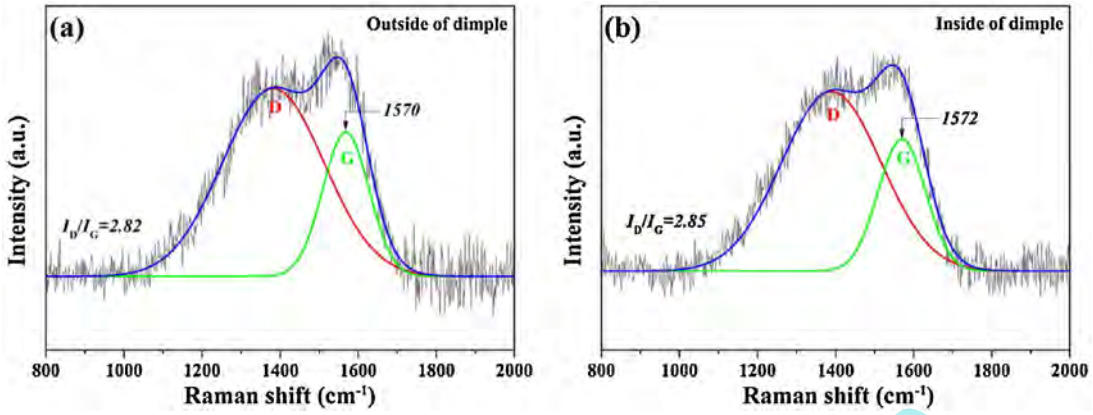

Fig. 4. Raman spectra of GLC-T30% obtained from (a) outside and (b) inside dimple.

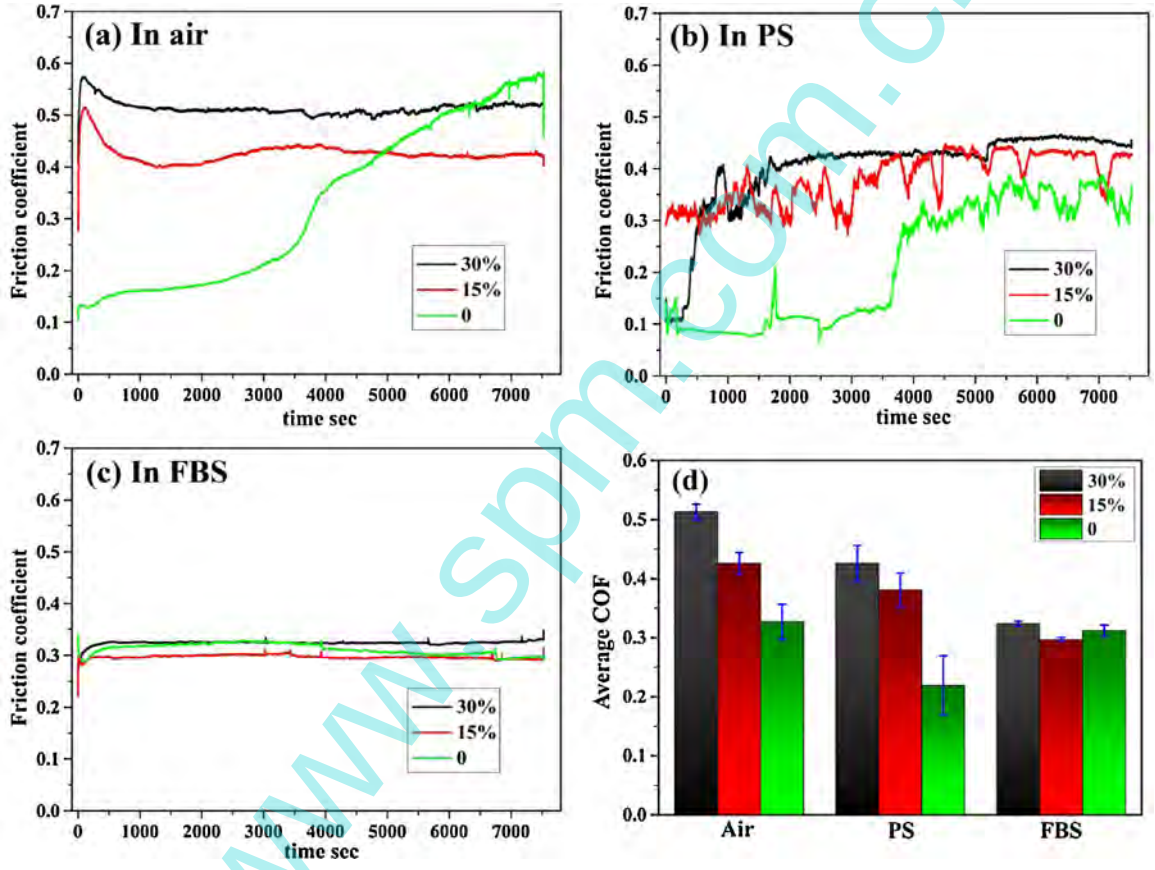

Fig. 5. COF curves and average COF of textured and un-textured PEEK in different medium: (a) in air, (b) in PS, (c) in FBS and (d) the corresponding of average COF.

suffers severe abrasion wear at the GLC/steel pin contact interface. The wear depth of un-textured GLC film is about 6 μm in air condition, which indicates the film has failed (combined with the thickness of GLC film in Fig. 1b). While the textured GLC film has narrower wear track and lower wear than that of un-textured one because micro-dimples can trap of wear debris at the contact interface to reduce abrasion wear of film. The element distribution of wear track is analyzed by energy dispersive X-ray (EDX) spectroscopy, as shown in Fig. S2 in Supporting information. The results demonstrate that silicon content (deriving from interlayer of film) of un-textured GLC film is very little, which verify the fact that un-textured GLC film is failed after 7200 s sliding time. While the textured GLC film has much silicon content in some regions, illustrating textured GLC film has a better wear resistance in air condition than that of un-textured one. In PS solution, the wear track of GLC coated PEEK is so shallow that the wear region is difficult to find (Fig. 8a). This is attributed to the synergistic effect of the fluid lubrication and surface passivation of water. In the FBS solution, the increasing temperature of contact surface will result in the thermal denaturation of protein, elongate the molecular chain of protein and increase the kinematic viscosity of relative motion [31]. In general, the thermal denaturation is an irreversible process. Even if the temperature is lowered again, the protein does not return to its original structure. However, the denatured protein at the interface as the lubrication layer can be effective to reduce the material wear. Thus, the morphology of wear track in FBS solution is very narrow, and the boundary line of wear track is not obvious. Therefore, GLC film can significantly improve the tribological

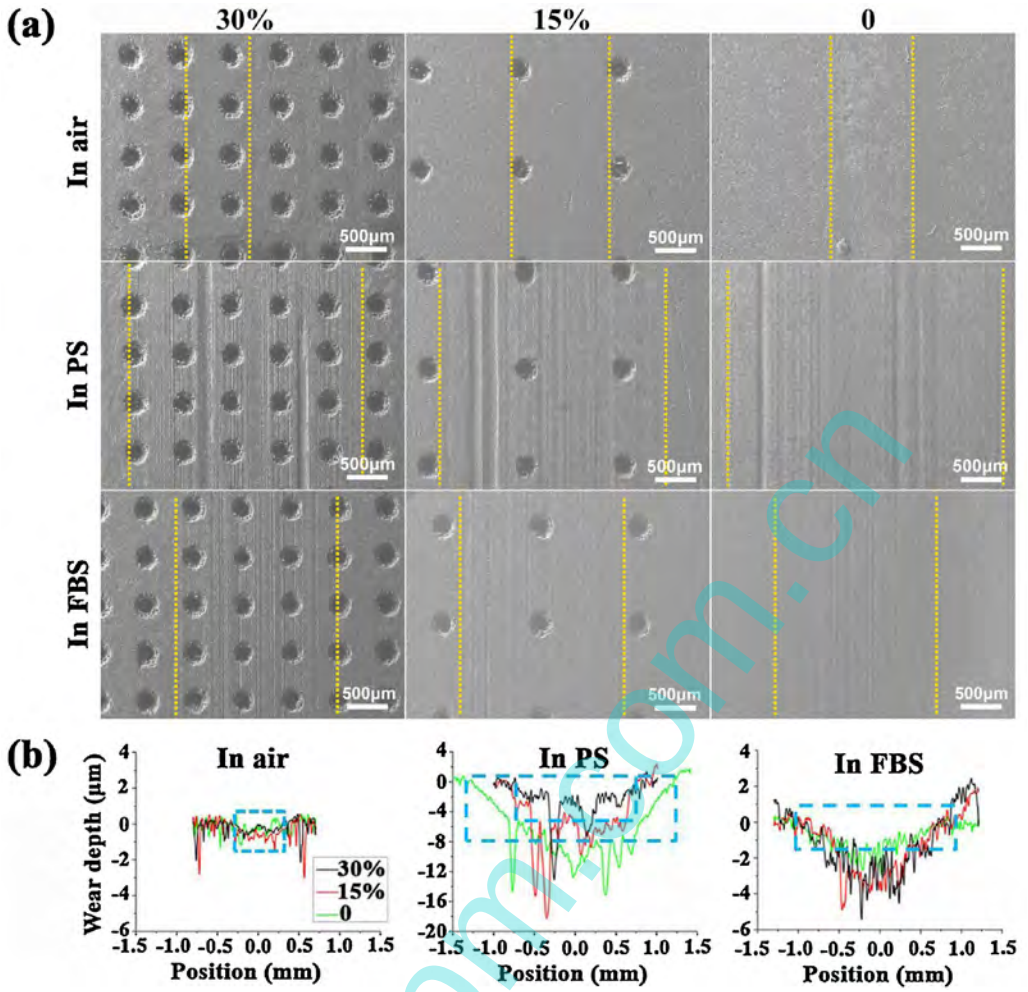

Fig. 6. (a) SEM images and (b) cross-section profiles of wear tracks for the textured and un-textured PEEK under different medium.

adaptive capability of PEEK in biological medium, and especially it greatly improves the wear-resistance of PEEK substrate. The wear is mainly seen as a smoothening effect of the outermost peaks of the surface roughness, which makes the determination of the wear volume extremely difficult (Fig. 8b). Moreover, titanium alloy and stainless steel substrate commonly used for orthopaedic applications are also tested in PS solution as a comparison with the wear resistance of GLC film. The results in Fig. S3 in Supporting information show that GLC film exhibits lower COF, and the wear resistance of GLC film is 1–2 orders of magnitude higher than that of titanium alloy and stainless steel.

Based on the above results, the friction and wear behaviours of the GLC film can be further explained. In air condition, most of strong dangling covalent σ-bonds from the GLC film and steel pin at the contact interface are terminated by C—H, C=O and COOH [40], which is attributed to the adsorption and dissociation effect of H_2O and O_2 from air. However, the relatively lack of water molecules in some contact areas leads to the formation of strong C—C covalent bonds, which increases the adhesion interaction between the GLC film and steel pin, thus resulting in a relatively higher COF and wear in air. When the specimen is tested in PS solution, the fluid lubricant provides plenty of water molecules and dissolved oxygen so that all of the dangling σ-bonds are almost terminated by C—H, C=O and COOH. Moreover, tribopair is not easy to contact each other owing to the existence of effective lubrication film. Therefore, the friction force is mainly derived from the interactions of hydrogen bonding and van der Waals force between tribopair and water, which is the main reason for the low friction and wear of GLC film in PS lubrication [31,41]. In FBS solution, the steady COF is higher than that in air and PS conditions (Fig. 7) whereas the wear is relative low (Fig. 8b), which is attributed to the fact that viscous protein easily sticks to the contact surface to form a continuous lubricated film. Fig. S4 in Supporting information shows the Raman spectra of the FBS solution and the transferred film on the wear scar against GLC-T30% in FBS solution. It confirms that much protein molecules are enriched in the wear scar region, which can protect the contact surface from rubbing each other. Moreover, friction force in FBS solution is not only from the interaction of hydrogen bonding and Van der Waals' force between the tribopair, but also derived from the viscous protein that has large molecular weight. Viscous protein with many interaction sites can form hydrogen bonding and van der Waals force with GLC film and its counterpart, which can increase the friction force between the tribopair [41]. Hence, in order to conquer the interaction sites between the sliding interface, a higher friction force must be applied at the sliding interface. Therefore, the COF in FBS solution is higher than that in PS solution.

According to the well-known Hamrock–Dowson formula for isoviscous-elastic lubrication in Eq. (1) [42], the corresponding lubrication regime can be approximately predicted according to the λ ratio in Eq. (2):

$$h_{\min} = 2.8R'\left(\frac{\eta\mu_e}{E'R'}\right)^{0.65}\left(\frac{W_y}{E'R'^2}\right)^{-0.21} \quad (1)$$

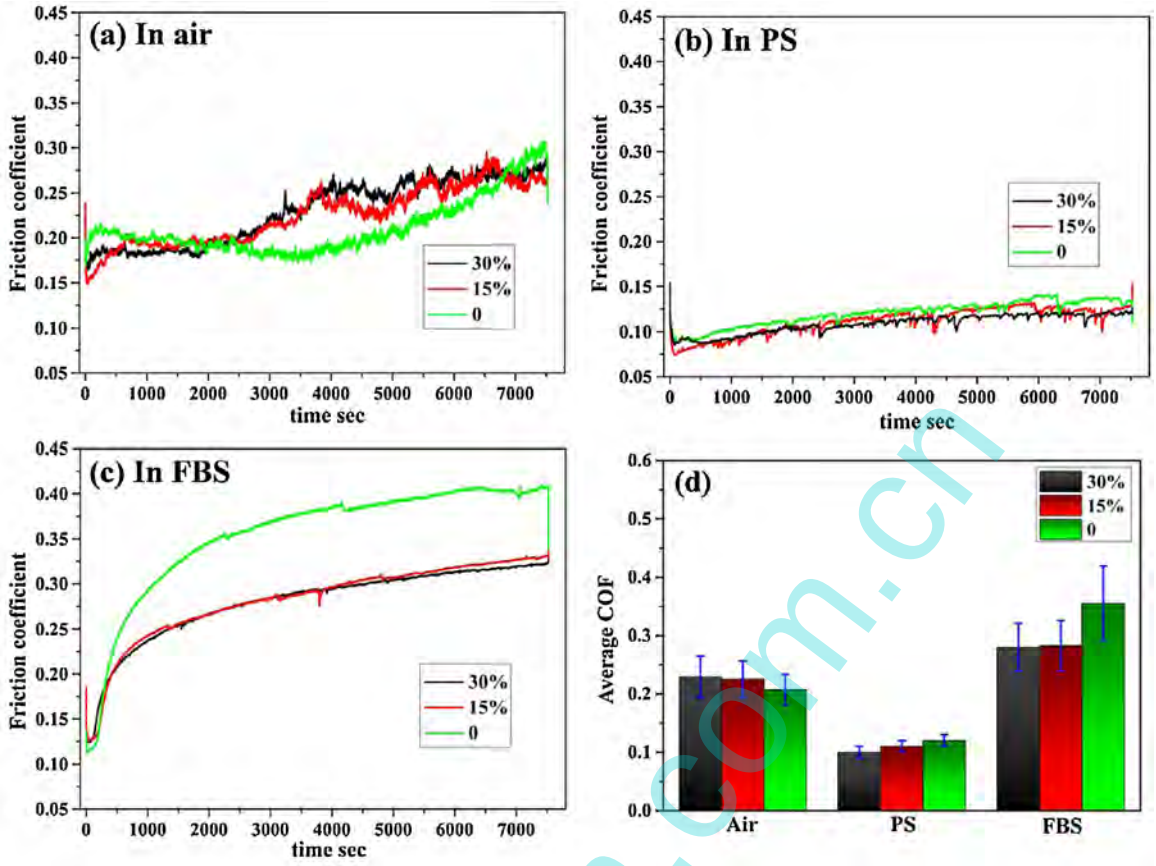

Fig. 7. COF curves and average COF of textured and un-textured GLC films in different medium: (a) in air, (b) in PS, (c) in FBS and (d) the corresponding of average COF.

Table 1
Mechanical properties of materials and typical roughness values for pin-on-plate configuration.

material	H (GPa)	E (GPa)	ν	R_a (μm)
pin: 316 L	7.0	193.1	0.3	0.02
plane: PEEK	0.2	3.6	0.25	0.14
plane: GLC	3.8	26.4	0.25	0.12

$$\lambda = \frac{h_{\min}}{R'_a} \tag{2}$$

$$R'_a = \sqrt{R_{a1}^2 + R_{a2}^2} \tag{3}$$

where $h_{\min}$ corresponds to the minimum film thickness, η is the lubricant viscosity, μ_e is the sliding velocity, W_y is the normal load, R'_a is the composite roughness, R' is the effective radius and E' is the elastic modulus.

$$R' = R_1 R_2/(R_2 - R_1) \tag{4}$$

$$\frac{1}{E'} = \frac{1}{2}\left(\frac{1-\nu_1^2}{E_1} + \frac{1-\nu_2^2}{E_2}\right) \tag{5}$$

where, R_1, E_1, ν_1 and R_2, E_2, ν_2, are the radii, Young's modulus and Poisson ratio of the pin and film, respectively. The specific parameters are reported in Table 1. According to the relevant parameters, $h_{\min}$ is figured out based on of Eq. (3), around 0.3 and 0.39 μm corresponding PS and FBS for PEEK substrate; around 0.13 and 0.17 μm corresponding PS and FBS for GLC film. Furthermore, Eq. (2) gives the λ ratio of 2.13 and 2.766 corresponding PS and FBS for PEEK substrate; gives the λ ratio of 1.065 and 1.393 corresponding PS and FBS for GLC film. It is commonly believed that the boundary lubrication mainly occur when the $0.1 < \lambda < 1$, mixed lubrication mainly occur when the $1 \leq \lambda \leq 3$ and $\lambda > 3$ is full film lubrication. Combined with the λ ratio meaning mixed lubrication may occur under these conditions. It's worth noting that tribochemical reactions are essential factor to determine the tribosystems running under boundary or mixed lubrication condition. Namely, the contact surface is in a mixed lubrication state that included hydrodynamic lubrication and asperity contacts simultaneously, and the corresponding COF can be expressed as [43]:

$$f = f_e k_e + f_l k_l \tag{6}$$

where f_e is the COF and k_e is the load carrying ratio of EHL film, f_l is the COF and k_l is the load carrying ratio of boundary lubrication film. In our experiments, when the texture density of PEEK is 15%, texture structure is helpful to reduce the COF of the specimen. It indicates that appropriate texture density can increase the roughness of PEEK to some extent, which is beneficial to form the EHL film and increases the thickness of EHL film, resulting in the decrease of the ratio k_e between the contact peak points [43]. And eventually, the integrated COF is also decreased. In contrast, when the texture density of PEEK is up to 30%, the ratio of minimum film thickness to the surface roughness is so small that the friction test is almost totally dominated by boundary lubrication regime. Consequently, the hydrodynamic effect from texture structure does not work and the contact pressure is almost loaded by the contact peak points, which leads the integrated COF of PEEK with 15% of texture density is lower than that of 30% (Fig. 5). However, the texture density has a little influence on GLC films under different medium. Only in PS solution, GLC-T30% exhibits a relatively lower COF than that of GLC-T15%. This finding can be explained by the function of the fluid/wear debris reservoirs of the dimples [30].

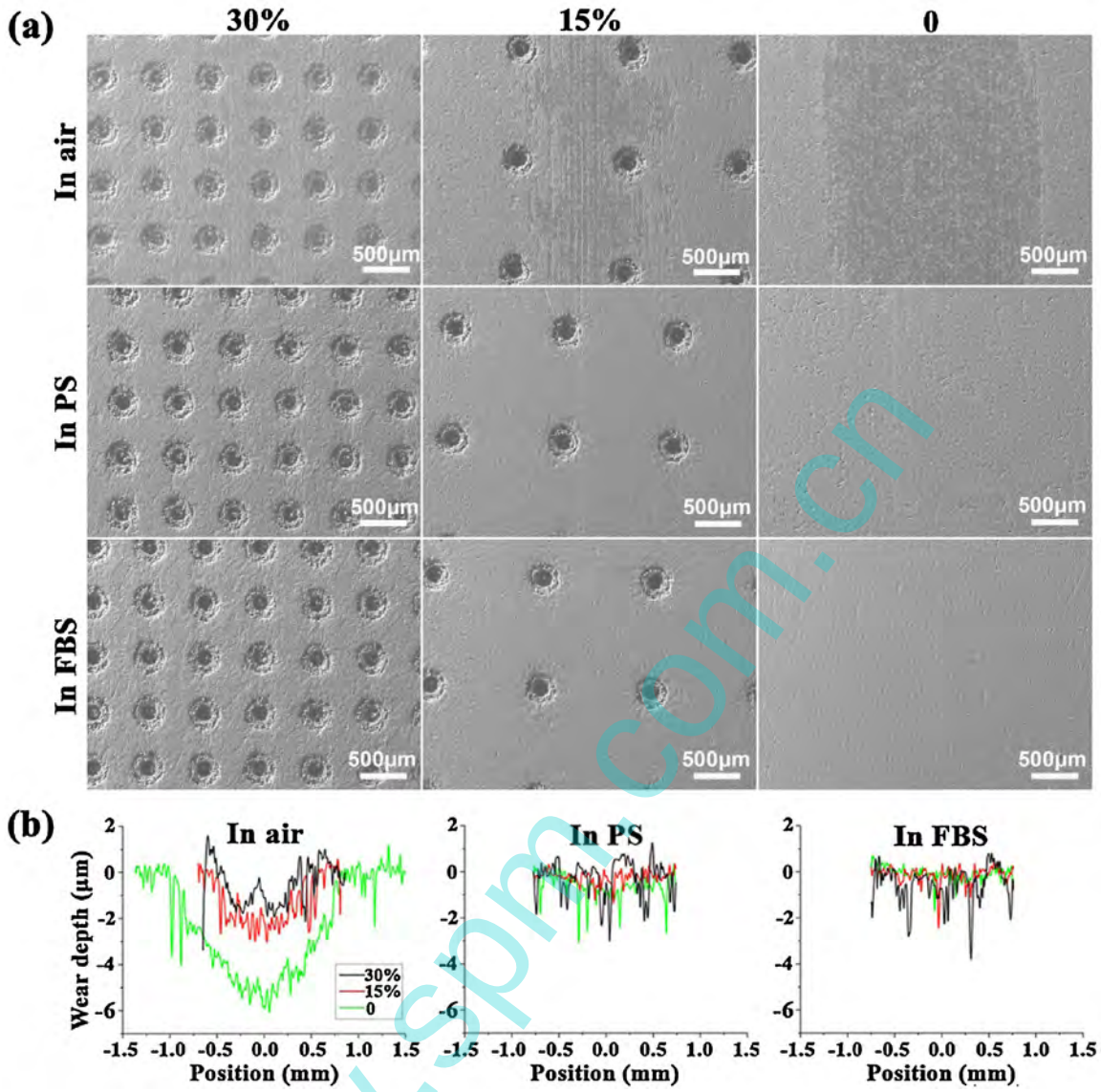

Fig. 8. (a) SEM images and (b) cross-section profiles of wear tracks for the textured and un-textured GLC films under different medium.

3.4. Evaluation of long lifetime for GLC film

With the developing of implant materials, careful consideration has been given to the longevity of the materials following many years implantation and the bioactivity of wear debris that may be generated from articulation. Fig. 9 shows the friction and wear behaviours of the GLC-T30% and un-textured GLC film against steel pins with the applied load of 3 N and 36,000 s of sliding (~229,320 cycles) in PS solution. Note that the un-textured GLC exhibits erratic COF while the COF of GLC-T30% stabilizes at a value between 0.09 and 0.11(Fig. 9a). Moreover, the COF of un-textured GLC film increases first and then decreases periodically to a stable value since the frictional heat consumes the solution gradually and causes the lack of solution, thus weakening hydrodynamic effects. When the fresh solution is added (two fresh droplets of the PS solution are brought in contact surface for each 7200 s sliding time), the COF stabilizes at a somewhat lower value of 0.12–0.13. While the GLC-T30% maintains a stable value at a whole test because the texturing surface can store more biological solution to provide hydrodynamic effects and result in low COF. Additionally, GLC films present an exceptional wear performance that the wear volumes are about 3.78×10^{-4} mm^3 for un-textured one and 2.60×10^{-4} mm^3 for GLC-T30% film (Fig. 9b). According to the literature [16], 10 million cycles represent approximately one decade of use for a typical elderly patient. Based on this result, it can be predicted that the wear volume of GLC-T30% after 10 million cycles is only about 0.011 mm^3, which is of great significant for developing textured GLC films as the long-period implant biomaterials. In terms of joint application, abrasive wear can produce relatively hard wear debris, which is undesirable [44]. Fortunately, GLC films present a smooth wear track and no groove can be found in Fig. 9c–f when these films experience ~229,320 sliding cycles. Meanwhile, the periphery of micro-dimples aggregates much of salt from PS solution (Fig. 9d and f) and the corresponding evidence of component analysis is shown in Fig. S5 in Supporting information, which confirms the presence of texture pattern can improve the capability of feeding PS solution into the sliding contact interface, thus isolating the wear particle.

3.5. Effect of load on the friction behaviour of textured GLC film

In human body, synovial joints are often subjected to external force, such as walking, running, and strenuous exercise. So, the effect of load on the friction behaviour of artificial implants

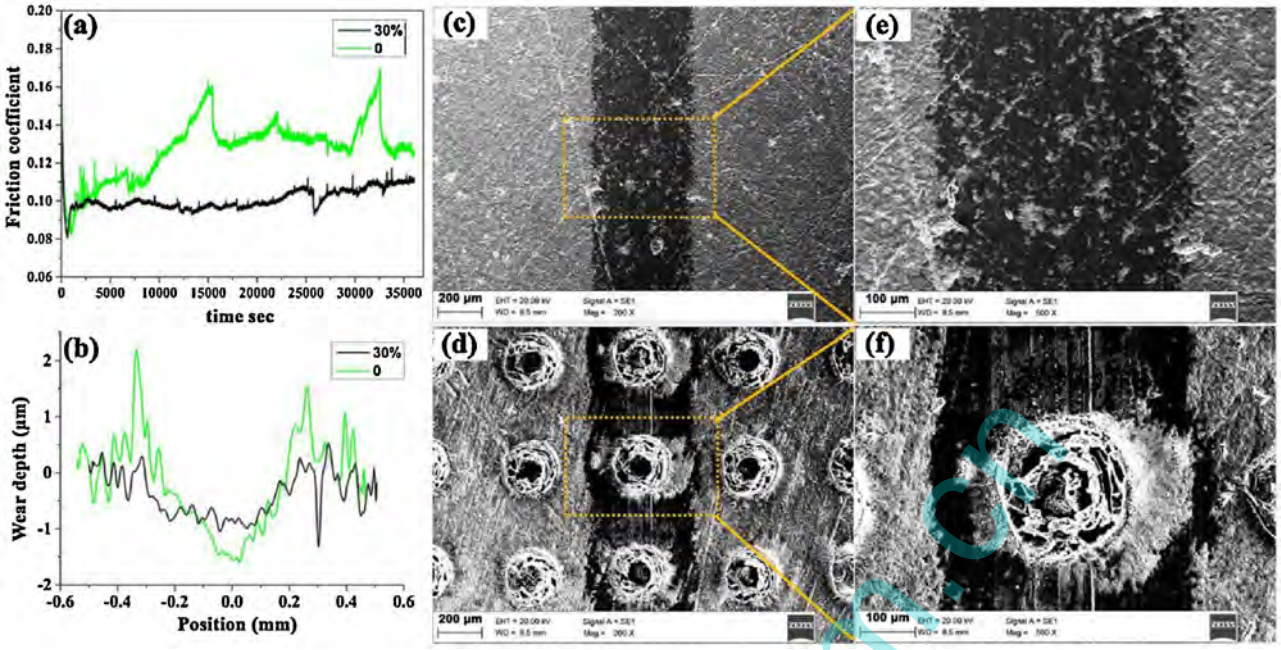

Fig. 9. Friction and wear behaviours of steel pin against textured and un-textured GLC films in PS solution: (a) Friction coefficient variation with time. (b) Cross-section profiles of wear track for GLC film after 36,000 s sliding time (~229,320 cycles). (c) The SEM image of wear track for the un-textured GLC film and (e) the corresponding to magnified image of selected area. (d) The SEM image of wear track for the textured GLC film and (f) the corresponding to magnified image of selected area.

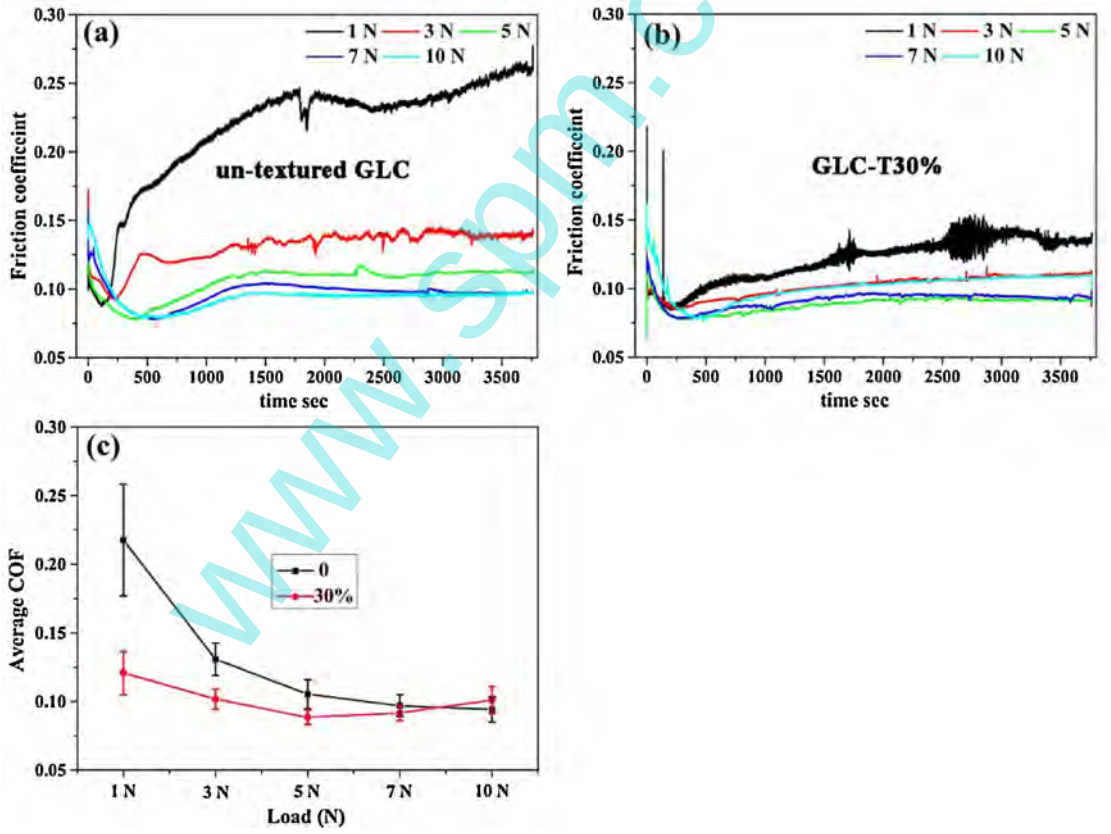

Fig. 10. COF curves and average COF of the graphite-like carbon film under different applied load: (a) un-textured GLC, (b) textured GLC, and (c) the corresponding of average COF.

is an essential factor to evaluate the lifetime of GLC film. In this study, the load of 1, 3, 5, 7 and 10 N is applied through a stationary loading system, and the corresponding initial maximum Hertzian contact pressure is about 0.15, 0.21, 0.25, 0.28 and 0.31 GPa, respectively. Fig. 10 shows the friction curves and the average COF of the un-textured GLC and GLC-T30% against the steel pin in PS solution under different applied load. Meanwhile, the average friction is measured for three times under the same load to calculate the

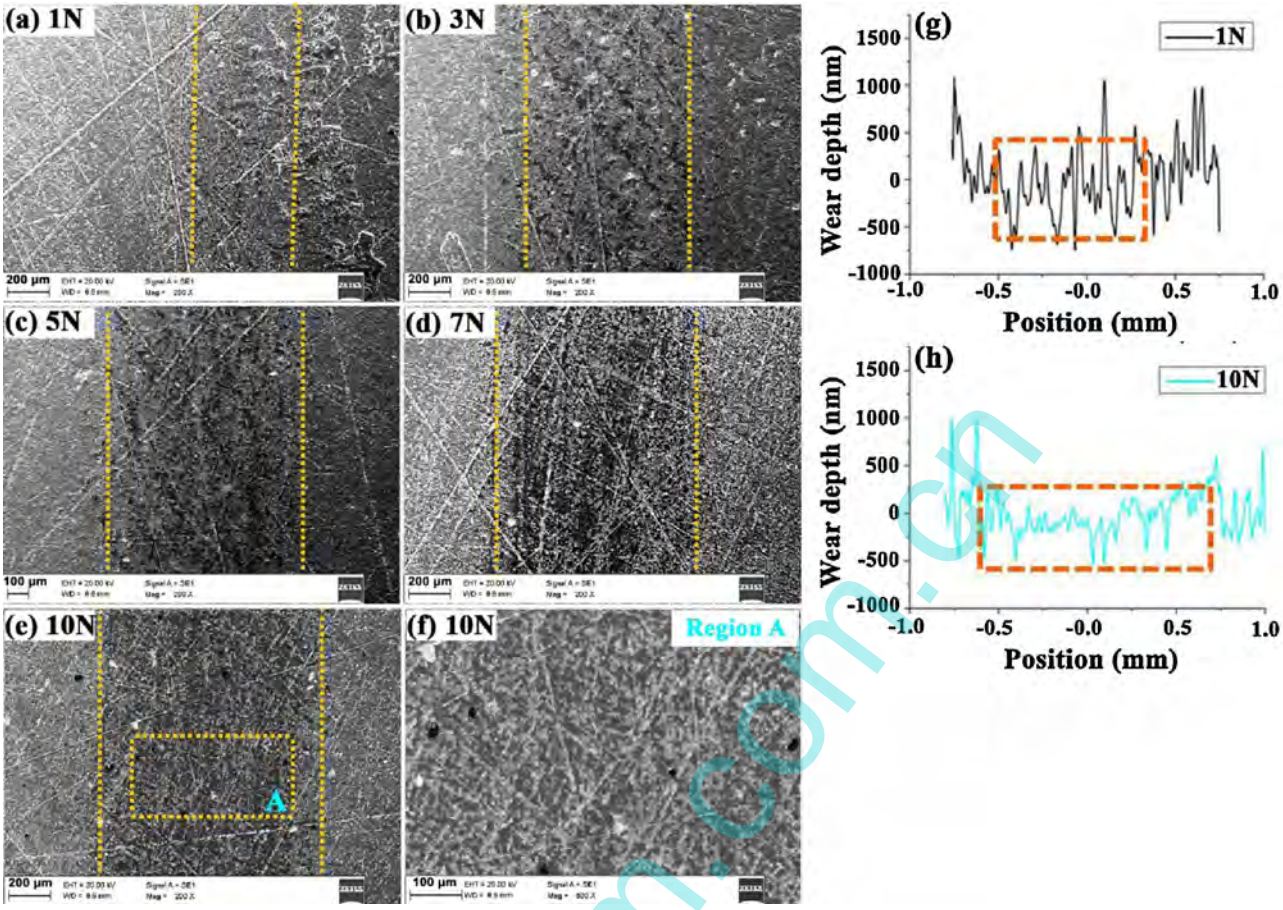

Fig. 11. (a–f) SEM images and (g, h) cross-section profiles of wear tracks for the un-textured GLC film at different applied load.

average value. The error bar is calculated from the standard deviation. As shown in Fig. 10, the applied load has a great influence on the tribological behaviour of un-textured and textured GLC films. For the un-textured GLC film (Fig. 10a), COF fluctuates with the increasing siding cycle under 1 N of applied load and the maximum value of COF reaches to the 0.27. With the increasing applied load, COF decreases to the minimum value of 0.09 and the friction curve is stable. The effect of load on the friction behaviour of un-textured GLC film can be divided into two stages. COF decreases with the increase in applied load obviously from 1 N to 5 N, which is described as the first stage. Subsequently, the decreasing tendency of COF is not obvious from 5 N to 10 N, which is described as the second stage. In addition, the COF of all un-textured GLC films is high at the initial sliding stage and decreases gradually with the increase in sliding cycle, and eventually attains the stable value. This is because mechanical interlocking, polishing micro-roughness and the establishment of transfer layer at running-in stage exist in the surface asperities between GLC film and counterpart steel pin, thus resulting in a high COF at this stage. With the increasing sliding cycle, asperities at the contact surface are polished, and the film material is transferred to counterpart surface to form a transfer layer. When a dense and continuous transfer layer is formed on the counterpart surface, COF reaches to the stable stage. For the GLC-T30% (Fig. 10b), COF is relatively high and fluctuant under 1 N of applied load, and the average COF reaches about 0.12. When the applied load rises to 5 N, COF is very stable and the average COF is about 0.08. However, when the load is up to 10 N, COF increases to 0.1, which indicates the high load is detrimental to form the EHL film. Moreover, the average COF of textured GLC is lower than that of un-textured GLC film (Fig. 10c), suggesting that surface texturing on the GLC film is beneficial to slow down the friction of human joint.

Generally speaking, the role of the single asperity can be ignored when the elastic deformation occurs at the contact surface. Thus the contact condition can be approximated as a sphere contacting with the plane. Based on the empirical formula: $f = CW^{-n}$ (where f is the friction coefficient, W is the normal load, $0 \leq n < 1/3$) [45], if the contact region is no plastic deformation, the contact area of a single asperity is proportional to $W^{2/3}$, and the COF is proportional to $W^{-1/3}$. When the contact region is in plastic deformation, the contact area of asperity is proportional to W. However, the elasto-plastic deformation coexists on the actual contact area and the corresponding COF is proportional to W^{-n}. Namely, COF decreases with the increase in applied load. The conclusion is in accord with the experiment for un-textured GLC film (Fig. 10a and c). But for textured GLC film, COF decreased first and increased afterward with the increase in applied load (Fig. 10b and c). According to Eq. (3), h_{min} is inversely proportional to the applied load W_y, while the texture surface of GLC film under a certain scope of loads can increase the thickness of fluid hydrodynamic film to avoid the direct contact of the asperities between the tribopair, thereby reducing the COF. When the applied load exceeds the critical value, the fluid hydrodynamic effect deriving from the texture structure can be weakened and the corresponding minimum film thickness (h_{min}) decreased, resulting in the increasing COF.

In order to further understand the tribological behaviour and wear mechanism of the textured GLC film in PS solution, the SEM morphologies and cross-section profiles of wear track of un-textured GLC film at different applied load are observed, as shown in Fig. 11. Under 1 N of applied load, the wear track is relatively

smooth and narrow, and the wear track line is difficulty to identify (Fig. 11a). The depth of wear track is not obvious and only scratched little micro-bugle of contact surface (Fig. 11f). With the increasing applied load, the wear track is still relatively smooth whereas the width of wear track increases and the shallow groove forms on the wear track. When the applied load rises to 10 N, the width of wear track increases to the maximum value and amounts of micro-bugle at the contact surface is grinded smoothly (Fig. 11e and h). As shown in Fig. 11f (marked region A in Fig. 11e), the wear track is mainly composed of alternation of "bright" and "dark" region, where the bright is the valley bottom and dark is the grinded peaks. This indicates that the wear mechanism of GLC film is mainly dominated by the plastic deformation.

Fig. 12 shows the SEM images and cross-section profiles of wear track of GLC-T30% at different applied load. As shown in Fig. 12, the wear track is relatively smooth and no evidence of wear or surface damage is observed under 1 N of applied load (Fig. 12a). With the increase in the applied load, the wear track is still relatively smooth whereas the width of wear track increased. Compared with un-textured GLC film (Fig. 11), the textured GLC film suffers a much lower wear under the same applied load. Indeed, in all the applied loads, the wear track line is hard to identify and the appearance of wear track does not change obviously as a comparison of fresh region. Therefore, we can safety conclude that the textured GLC film exhibits excellent tribological performance under biological environment. However, when we look over the morphology of wear track for GLC-T30%, an interesting phenomenon is found that the wear of textured GLC film mainly occurs on the edge of micro-dimples and terminated on the central between two adjacent micro-dimples. This phenomenon is more evident at the 10 N of applied load. Based on cross-section profile of wear track (Fig. 12g), there is no obvious difference on the depth of wear track on the central regions (just like region A in Fig. 12a) before and after sliding tests, which confirms that wear mainly occurs on the edge of micro-dimples because of its higher roughness than central regions. This higher roughness results from the plastic deformation during laser texturing. Moreover, Ding et al. [43] consider that the central region between micro-dimples is unenhanced electrical fields area where the film has a low sp^2 content and high hardness. But the edge of micro-dimples is the reinforcement of local electrical fields where the sp^2 content increases and the hardness decreases with the decrease in the distance between micro-dimples. Namely, the textured GLC film possesses a soft-hard alternating structure and hardness gradient at the lateral direction. This structure is beneficial to release the internal stress of film and then prevents the stress concentration and the crack generation. So, the edge of micro-dimples on the wear track is only slight plastic deformation without grooves or crack, as shown in Fig. 12f.

To take a closer look at the contact state between the pin and GLC film, we calculate plasticity indices to estimate the deformation extent of micro asperities and qualitatively predict the contact is elastic or plastic. The plasticity index is given by GW model in Eq. (7) [43,46]:

$$\varphi = (E*/H)(\sigma_s k_s)^{1/2} \quad (7)$$

$$1/E* = (1-\nu_1^2)/E_1 + (1-\nu_2^2)/E_2 \quad (8)$$

where H is the hardness of softer material for tribopair, E^* is reduced Young's modulus, σ_s is the composite roughness that calculates by Eq. (3), and k_s is the curvature constant that obtains by optical profiler ($k_s \approx 1.2 \times 10^{-4}$ nm^{-1}). Combining the mechanical properties of the steel pin and un-textured GLC film in Table 1 as well as the surface morphology parameters, the plasticity index is calculated about 0.75 according to above equations. The contact state is commonly identified by the following ranges: $\varphi < 0.6$ is classified into elastic deformation whereas $\varphi > 1$ is classified into plastic deformation. This indicates the contact state between steel pin and GLC is mainly elastic deformation mixed with a small portion of plastic deformation, which confirms the present experimental results in Figs. 11 and 12.

Fig. 13 shows the optical observation of wear scars on the mating pins against GLC-T30% film in PS solution at 1 N and 10 N of applied load. As shown in Fig. 13a, the wear scar is surrounded by a number of loose debris but no transfer layer is formed under 1 N of applied load, which can be used to explain the fluctuant COF (Fig. 10b). With the increasing applied load, the central region of wear scar aggregates some transfer layer and amounts of debris is gathered around the edge of wear scar. The formed transfer layer avoids the direct contact of GLC film and steel pin, effectively reducing the shear force at the contact interface.

In order to investigate the GLC phase transformation during friction, Raman spectroscopy is performed (Fig. 14). Compared with G peak (1570 cm^{-1}) of as-deposited GLC film (Fig. 4), G peak of wear scar against GLC-T30% under low load (1 N) and high load (10 N) shifts 1575 cm^{-1} and 1585 cm^{-1}, respectively, as shown in Fig. 14a and b. Meanwhile, D band becomes more evident and the intensity ratio I_D/I_G for low load and high load goes up from 2.82 to 2.90 and 3.23, respectively. As proposed by Ferrari and Robertson [47], it can conclude that the as-deposited GLC film has been graphitized during the friction. Moreover, the Raman shift of G-band and the I_D/I_G ratio under the heavy load is higher than that under light load, suggesting that the contact pressure is an important factor in inducing graphitization. However, the I_D/I_G ratio of un-textured GLC film (Fig. 14c and d, I_D/I_G ~2.92 for 1 N and ~3.92 for 10 N) is higher than that of GLC-T30% under the same load, indicating that the texture structure is an important factor in inhibiting graphitization. Therefore, the higher wear of un-textured GLC film can be attributed to the formation of graphite layer on the contact surface [48]. Particularly, the relatively soft graphite layers are more prone to reduce the COF due to the low shear-strength of itself. It explains why the COF decreases with the increase in the applied load.

In combination with the above analysis, the friction and wear mechanism of GLC film under PS solution can be described in Fig. 15. The surface of GLC has amounts of micro-asperities. When the liquid lubricant spreads uniformly on the surface of film, the large asperities in some place can be protruded the outside of lubricant film where the liquid film is thinner than others. Therefore, two lubricating regions involving partial fluid-lubricated regions and solid-solid contact regions in micro-scale may coexist on the contact surface. Under the low load, only small amounts of asperities are worn away by mechanical abrasive at the initial friction stage due to the high hardness of GLC film. It is not easy to form a continuous transfer layer but only accompanied with a fluid film under the low contact pressure. With the increase in the applied load, contact area increases with the increase in sliding cycle, and amounts of wear debris are generated to form a transfer layer which is caused by the fact that high contact pressure accelerates the chemical reactivity between tribopair. The formed transfer layer is thin and not continuous at the initial stage but it also can play a role in reducing friction [49]. With the increasing sliding distance, a continuous, uniform and dense transfer film is formed on the steel pin, further reducing COF. Meanwhile, a wear induced graphitization process takes place which facilitates low friction, leading to the COF decreases with the increase in applied load. However, for the textured GLC film, the texture structure can capture more liquid lubricant, which is beneficial to increase the thickness of EHL film. The EHL film can reduce the COF, improve the resistance to plastic deformation for the GLC film and decrease the indentation deformation for the counterpart pin, thus improving wear resistance of film. In contrast with un-textured GLC film, textured GLC film experiences a much lower graphitization owing to the trapping wear debrisof micro-dimples, which is helpful for the maintenance

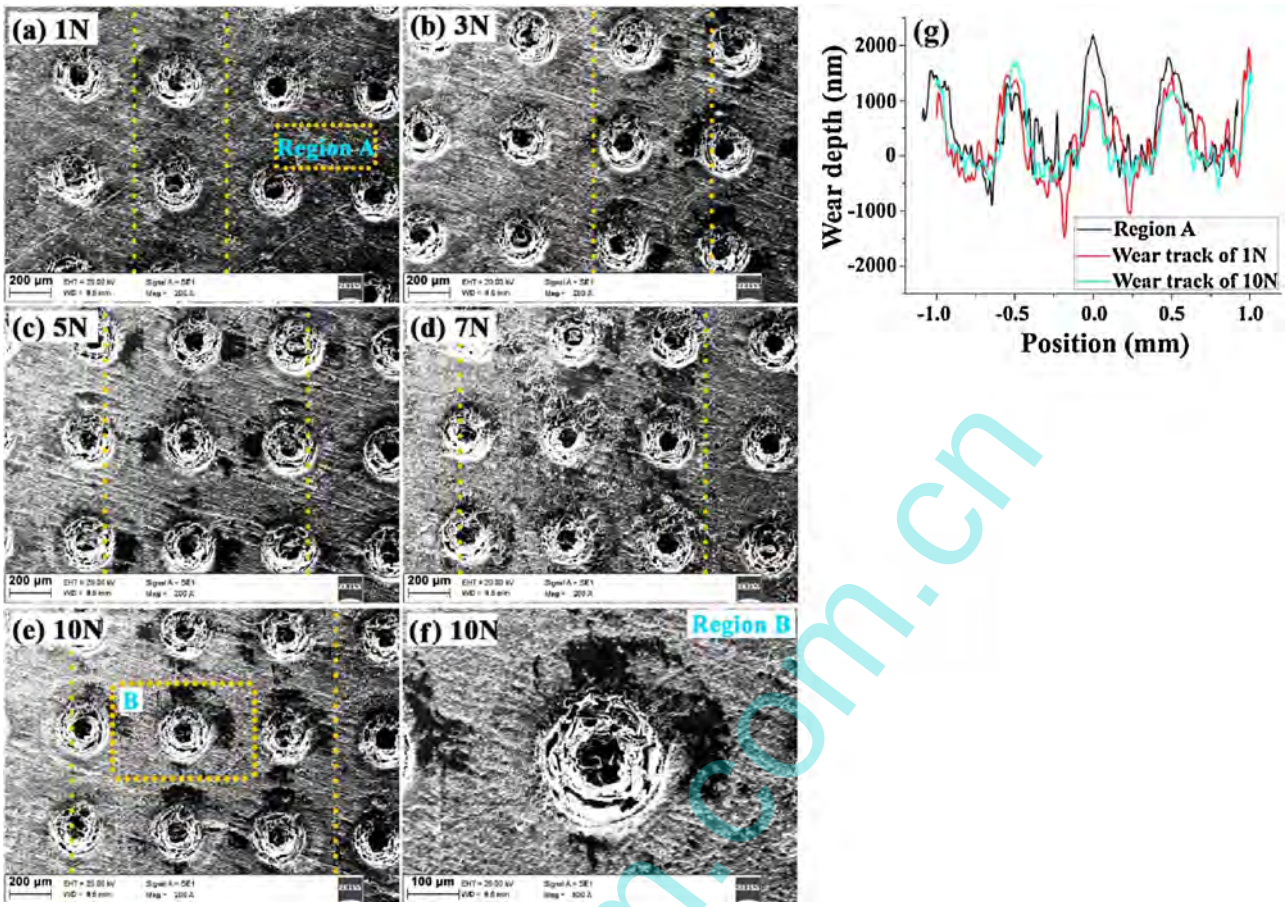

Fig. 12. (a–f) SEM images and (g) cross-section profiles of wear tracks for the GLC-T30% at different applied load.

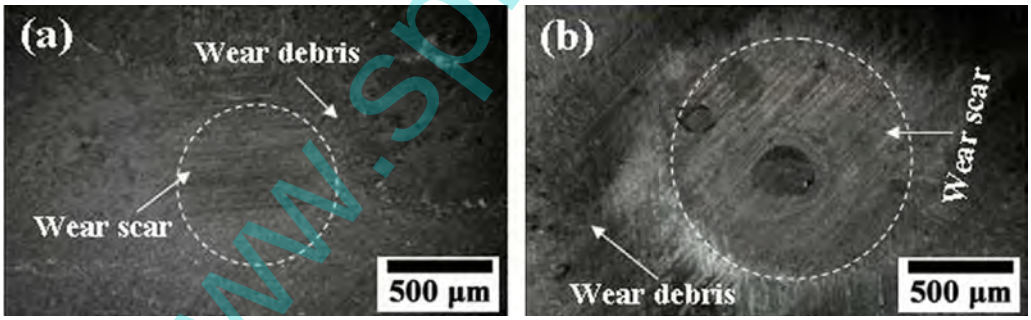

Fig. 13. Optical observation of wear scars of the mating pins against GLC-T30% film in PS solution at (a) 1 N and (b) 10 N of applied load.

of film hardness during whole test [43]. Therefore, the textured GLC film has a better wear resistance than the film with smooth structure. When the applied load rises to 10 N, the COF of textured GLC film is higher than that of un-textured GLC film, which can be attributed to the fact that the extra hydrodynamic effect caused by surface texture is diminished. Above all, the textured GLC-based solid-liquid synergistic lubrication films are required for the potential application in implant replacements.

4. Conclusions

In summary, we have studied the effects of the texturing surface on the friction and wear behaviours of PEEK with GLC film in ambient air and biochemical fluid, and discussed the relationship of friction and wear with contact pressure. The findings indicated that the GLC film modified PEEK substrate could exhibit remarkable friction reduction and antiwear performance in PS and FBS conditions, suggesting the GLC film had more advantages for the surface protection of PEEK. Particularly, no groove was observed at the wear track of GLC coated PEEK in PS solution, which was only accompanied with slight plastic deformation. Moreover, 15% of texture density for PEEK had a lower COF than those with 30% under simulated body fluid conditions. The texture density for GLC film had a little influence for friction performance. Only in case of PS solution, the GLC-T30% exhibited a relatively lower COF than that of GLC-T15%. Furthermore, the applied load had a great influence on the tribological behaviour of un-textured and textured GLC films in PS solution. The COF of un-textured and textured GLC films decreased with the increase in applied load. And the textured GLC film had a better friction reduction performance than that of un-textured GLC under different applied load, which was attributed to the fact that the texture surface could induce the hydrodynamic

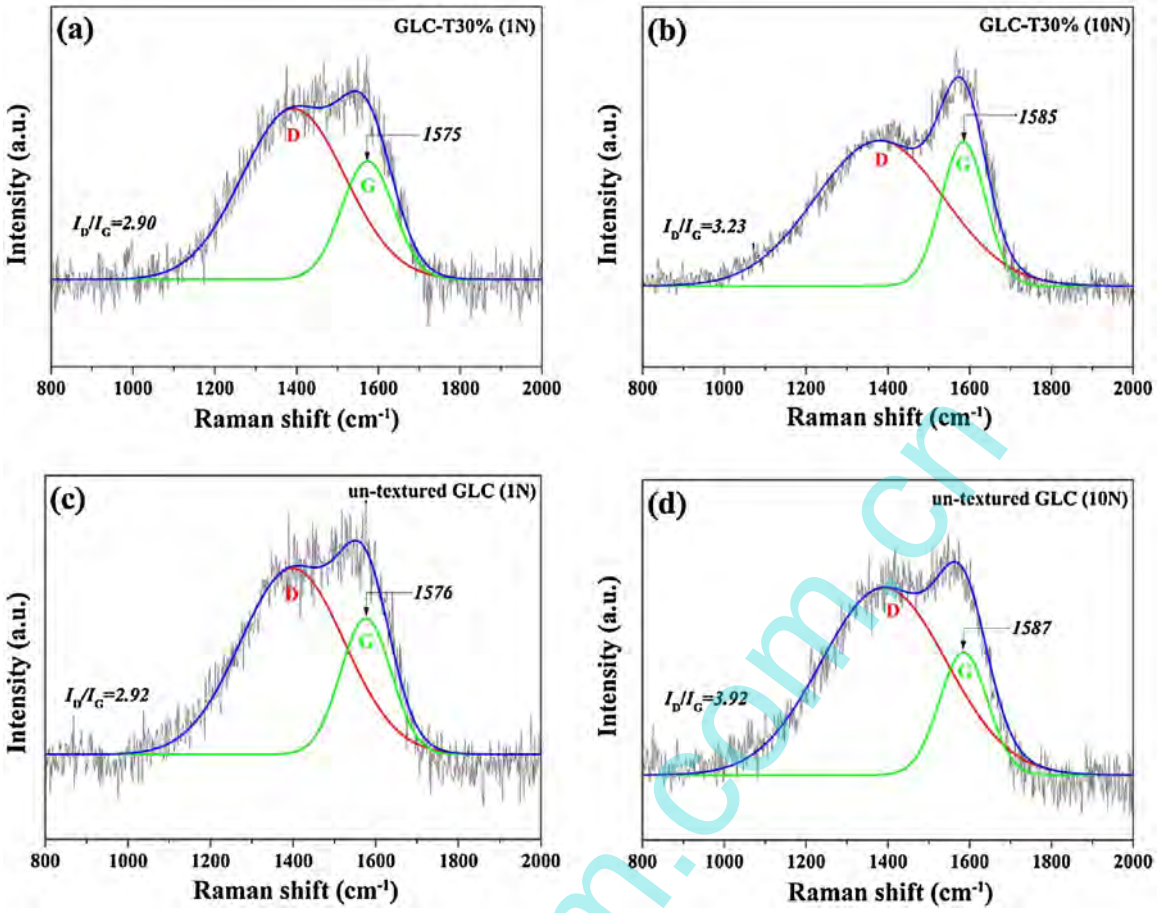

Fig. 14. Raman spectra of the transferred films on the wear scar against GLC-T30% in PS solution at (a) 1 N and (b) 10 N of applied load as well as against un-textured GLC film at (c) 1 N and (d) 10 N of applied load.

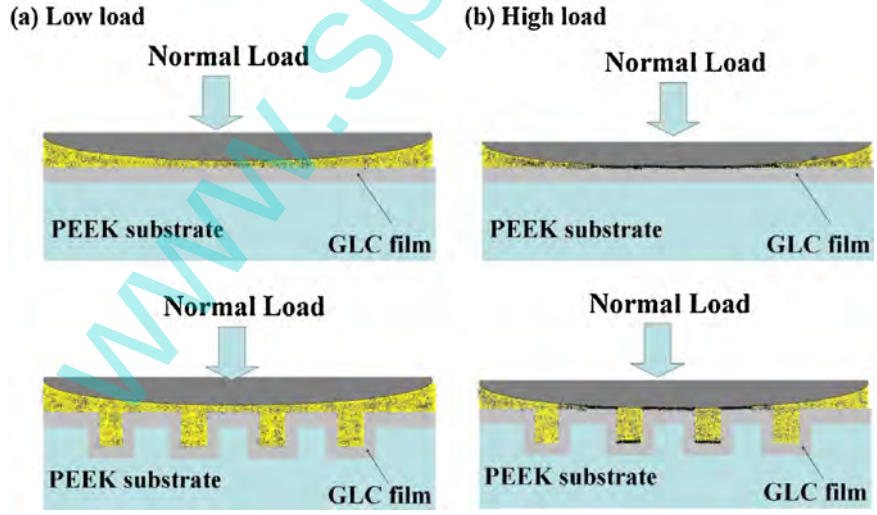

Fig. 15. Schematic diagram of the effects of surface texturing on phase transformation during friction for: (a) low load, (b) high load.

effect to increase the thickness of EHL film. Meanwhile, with the increasing applied load, the textured GLC film experienced a much lower graphitization than that of un-textured GLC due to the trapping wear debris effect of texture surface which was helpful for the maintenance of film hardness during whole test.

Acknowledgements

The authors are grateful for financial support from the National Key Basic Research Program (No.2014CB643302), the National Natural Science Foundation of China (No.41506098), and the ZheJiang Provincial Natural Science Foundation of China.

Appendix A. Supplementary data

Supplementary data associated with this article can be found, in the online version, at http://dx.doi.org/10.1016/j.apsusc.2016.12.159.

References

[1] T. Murakami, H. Higaki, Y. Sawae, N. Ohtsuki, S. Moriyama, Y. Nakanishi, Adaptive multimode lubrication in natural synovial joints and artificial joints, Proc. Inst. Mech. Eng. Part H: J. Eng. Med. 212 (1998) 23–35.
[2] M. Long, H.J. Rack, Titanium alloys in total joint replacement-a materials science perspective, Biomaterials 19 (1998) 1621–1639.
[3] D. Dowson, Bio-tribology of natural and replacement synovial joints, Biomech. Diarthrodial Jt. 2 (1990) 303–345.
[4] E.W. Lowman, Osteoarthritis, J. Am. Med. Assoc. 157 (1955) S6.
[5] J. Black, Biological Performance of Materials, Marcel Dekker, New York, 1992.
[6] J.A. Disegi, L. Eschbach, Stainless steel in bone surgery, Injury 31 (2000) D2–D6.
[7] E. Ingham, J. Fisher, Biological reactions to wear debris in total joint replacement, Proc. Inst. Mech. Eng. Part H, J. Eng. Med. 214 (2000) 21–37.
[8] L. Eschbach, Nonresorbable polymers in bone surgery, Injury 31 (2000) D22–D27.
[9] M. Akay, N. Aslan, Numerical and experimental stress analysis of a polymeric composite hip joint prosthesis, J. Biomed. Mater. Res. 31 (1996) 167–182.
[10] M.F. Talbott, G.S. Springer, L.A. Berglund, The effects of crystallinity on the mechanical properties of PEEK polymer and graphite fiber reinforced PEEK, J. Compos. Mater. 21 (1987) 1056–1081.
[11] Z.P. Lu, K. Friedrich, On sliding friction and wear of PEEK and its composites, Wear 181 (1995) 624–631.
[12] K. Fujihara, Z.M. Huang, S. Ramakrishna, K. Satknanantham, H. Hamada, Performance study of braided carbon/PEEK composite compression bone plates, Biomaterials 24 (2003) 2661–2667.
[13] J. Huang, S. Wan, B. Liu, Q. Xue, Improved adaptability of PEEK by Nb doped graphite-like carbon composite coatings for bio-tribological applications, Surf. Coat. Technol. 247 (2014) 20–29.
[14] A. Wang, R. Lin, C. Stark, J.H. Dumbleton, Suitability and limitations of carbon fiber reinforced PEEK composites as bearing surfaces for total joint replacements, Wear 225 (1999) 724–727.
[15] T.J. Joyce, C. Rieker, A. Unsworth, Comparative in vitro wear testing of PEEK and UHMWPE capped metacarpophalangeal prostheses, Bio-Med. Mater. Eng. 16 (2006) 1–10.
[16] S.M. Kurtz, J.N. Devine, PEEK biomaterials in trauma, orthopedic, and spinal implants, Biomaterials 28 (2007) 4845–4869.
[17] P.E. Purdue, P. Koulouvaris, B.J. Nestor, T.P. Sculco, The central role of wear debris in periprosthetic osteolysis, HSS J. 2 (2006) 102–113.
[18] L. Wang, X. Guan, G. Zhang, Friction and wear behaviors of carbon-based multilayer coatings sliding against different rubbers in water environment, Tribol. Int. 64 (2013) 69–77.
[19] H.A. Ching, D. Choudhury, M.J. Nine, N.A.A. Osman, Effects of surface coating on reducing friction and wear of orthopaedic implants, Sci. Technol. Adv. Mater. 15 (2014) 506–512.
[20] N.A. Peppas, R. Langer, New challenges in biomaterials, Science 263 (1994) 1715–1719.
[21] S.B. Goodman, Wear particles, periprosthetic osteolysis and the immune system, Biomaterials 28 (2007) 5044–5048.
[22] S.C. Kwok, P. Yang, J. Wang, X. Liu, P.K. Chu, Hemocompatibility of nitrogen-doped, hydrogen-free diamond-like carbon prepared by nitrogen plasma immersion ion implantation–deposition, J. Biomed. Mater. Res. Part A 70 (2004) 107–114.
[23] R. Hauert, K. Thorwarth, G. Thorwarth, An overview on diamond-like carbon coatings in medical applications, Surf. Coat. Tech. 233 (2013) 119–130.
[24] J. Huang, S. Wan, L. Wang, Q. Xue, Tribological properties of Si-doped graphite-like amorphous carbon film of PEEK rubbing with different counterparts in SBF medium, Tribol. Lett. 57 (2015) 1–9.
[25] A. Ramesh, W. Akram, S.P. Mishra, A.H. Cannon, A.A. Polycarpou, W.P. King, Friction characteristics of microtextured surfaces under mixed and hydrodynamic lubrication, Tribol. Int. 57 (2013) 170–176.
[26] C. Zhao, X. Xiang, L. Guo, S. Wei, L. Ying, Texture structure and ablation behavior of TaC coating on carbon/carbon composites, Appl. Surf. Sci. 257 (2010) 656–661.
[27] N.P. Suh, M. Mosleh, P.S. Howard, Control of friction, Wear 175 (1994) 151–158.
[28] I. Etsion, Improving Tribological performance of mechanical components by laser surface texturing, Tribol. Lett. 17 (2004) 733–737.
[29] A. Kovalchenko, O. Ajayi, A. Erdemir, G. Fenske, I. Etsion, The effect of laser texturing of steel surfaces and speed-load parameters on the transition of lubrication regime from boundary to hydrodynamic, Tribol. Trans. 47 (2004) 299–307.
[30] D. He, S. Zheng, J. Pu, G. Zhang, L. Hu, Improving tribological properties of titanium alloys by combining laser surface texturing and diamond-like carbon film, Tribol. Int. 82 (2015) 20–27.
[31] J. Huang, L. Wang, B. Liu, S. Wan, Q. Xue, In vitro evaluation of the tribological response of Mo-doped graphite-like carbon film in different biological media, ACS Appl. Mater. Interfaces 7 (2015) 2772–2783.
[32] X. Wang, P. Wang, S. Yang, J. Zhang, Tribological behaviors of fullerene-like hydrogenated carbon (FL-C:H) film in different atmospheres sliding against Si_3N_4 ball, Wear 265 (2008) 1708–1713.
[33] G. Zhang, P. Yan, P. Wang, Y. Chen, J. Zhang, The preparation and mechanical properties of Al-containing a-C:H thin films, J. Phys. D: Appl. Phys. 40 (2007) 6748.
[34] S. Wan, H. Hu, G. Chen, J. Zhang, Synthesis and characterization of high voltage electrodeposited phosphorus doped DLC films, Electrochem. Commun. 10 (2008) 461–465.
[35] S.K. Field, M. Jarratt, D.G. Teer, Tribological properties of graphite-like and diamond-like carbon coatings, Tribol. Int. 27 (2004) 949–956.
[36] A.C. Ferrari, J. Robertson, Raman spectroscopy of amorphous, nanostructured, diamond–like carbon, and nanodiamond, Philos. Trans. R. Soc. Lond. A: Math. Phys. Eng. Sci. 362 (2004) 2477–2512.
[37] G. Cantero, A. Arbelaiz, R. Llano-Ponte, I. Mondragon, Effects of fibre treatment on wettability and mechanical behaviour of flax/polypropylene composites, Compos. Sci. Technol. 63 (2003) 1247–1254.
[38] J.K. Lancaster, Lubrication of carbon fibre-reinforced polymers part I—water and aqueous solutions, Wear 20 (1972) 315–333.
[39] Z. Yang, Y. Fujii, F.K. Lee, C.H. Lam, O.K. Tsui, Glass transition dynamics and surface layer mobility in unentangled polystyrene films, Science 328 (2010) 1676–1679.
[40] C. Donnet, D. Erdemir, Tribology of Diamond-Like Carbon Films: Fundamentals and Applications, Springer, New York, USA, 2008, pp. 155–200.
[41] R.Q. Hang, Y. Qi, A study of biotribological behavior of DLC coatings and its influence to human serum albumin, Diam. Relat. Mater. 19 (2010) 62–66.
[42] Z.M. Jin, D. Dowson, J. Fisher, Analysis of fluid film lubrication in artificial hip joint replacements with surfaces of high elastic modulus, Proc. Inst. Mech. Eng. Med. 211 (1997) 247–256.
[43] Q. Ding, L. Wang, Y. Wang, S.C. Wang, L. Hu, Q. Xue, Improved tribological behavior of DLC films under water lubrication by surface texturing, Tribol. Lett. 41 (2011) 439–449.
[44] B. Shi, O.O. Ajayi, G. Fenske, A. Erdemir, H. Liang, Tribological performance of some alternative bearing materials for artificial joints, Wear 255 (2003) 1015–1021.
[45] E. Liu, B. Blanpain, J.P. Celis, J.R. Roos, Comparative study between macrotribology and nanotribology, J. Appl. Phys. 84 (1998) 4859–4865.
[46] A. Kumar, T. Staedler, X. Jiang, Effect of normal load and roughness on the nanoscale friction coefficient in the elastic and plastic contact regime, Beilstein J. Nanotechnol. 4 (2013) 66–71.
[47] A.C. Ferrari, J. Robertson, Interpretation of Raman spectra of disordered and amorphous carbon, Phys. Rev. B Condens. Matter 61 (2000) 14095–14107.
[48] S. Ren, S. Zheng, J. Pu, Z. Lu, G. Zhang, Study of tribological mechanisms of carbon-based coatings in antiwear additive containing lubricants under high temperature, RSC Adv. 5 (2015) 66426–66437.
[49] C. Kajdas, Importance of anionic reactive intermediates for lubricant component reactions with friction surfaces, Lubr. Sci. 6 (1994) 203.